Can Tho University Journal of Science
website: ctujs.ctu.edu.vn

DOI: 10.22144/ctu.jen.2022.015

Preparation of Fe_3O_4/HAp nanoparticles from eggshells with highly adsorption capacity for methylene blue

Luong Huynh Vu Thanh[1,2*], Nguyen Ngoc Han[1], Khuu Gia Han[1], Bui Yen Pha[1], Thieu Quang Quoc Viet[2], Ngo Truong Ngoc Mai[2], and Tran Thi Bich Quyen[2]

[1]*Applied Chemical Engineering Lab, College of Engineering Technology, Can Tho University, Viet Nam*

[2]*Department of Chemical Engineering,* College of *Engineering Technology, Can Tho University, Viet Nam*

**Correspondence: Luong Huynh Vu Thanh (email: lhvthanh@ctu.edu.vn)*

Article info.

Received 10 Feb 2022
Revised 20 Mar 2022
Accepted 20 Jun 2022

Keywords

Adsorption, eggshell, methylene blue, nano Fe_3O_4@HAp

ABSTRACT

Multifunctional materials have become one of the most interesting research subjects in recent years. Hydroxylapatite (HAp) coating on the surface of iron oxide (Fe_3O_4) nanoparticles allow to obtain material with adsorbable and magnetic properties. This study aims to salvage recycled eggshell to successfully produce adsorbent nanoparticles and evaluate treatment ability of methylene blue (MB) dyes in water. The magnetic nanomaterial was synthesized by a simple and inexpensive method. The X-ray diffraction technique was employed to characterize the structure of nanoparticles. The as-synthesized nanoparticles were analyzed by Fourier transform infrared spectroscopy technique to determine the presence of functional groups and bonds in the molecule. The surface morphology of as-synthesized Fe_3O_4/HAp nanoparticles was studied by transmission electron microscopy. The magnetic properties of Fe_3O_4 nanoparticles and Fe_3O_4/HAp nanoparticles were evaluated by vibrating sample magnetometer technique. The typical synthesized-HAp were dispersed rod-like particles with about 10 nm in width and 50 nm in length, the other part of final material was dispersed in spherical shape and their magnetism was 16.2 emu.g^{-1}. The adsorption of MB was conducted with 89.6% yield at pH 8.

1. INTRODUCTION

The development of industrialization leads to increases in environmental pollution, especially dye pollutants in the aquatic environment, which poses serious threats to public health and ecological systems. Among the pollutants of concern, methylene blue (MB) has been considered as one of the major water environmental pollutants, it predominates in surface water and groundwater. Because of the negative effects of MB, its removal from water is an urgent matter. Many studies to find solutions to treat water supply and wastewater have been carried out. Techniques to remove MB from wastewater include biological treatment (El-Naas et al., 2009), coagulation (El-Gohary & Tawfik, 2009), redox (Gomes et al., 2008), membrane filtration technology (Dâas & Hamdaoui, 2010), and a combination of many other methods (Wu et al., 2011). However, adsorption is probably the most common method in practical use thanks to its simplicity and high efficiency as well as versatility and suitability for most practical wastewater treatment processes.

Fe_3O_4 is a material with high potential applications in many fields. In this study, the main purpose of using Fe_3O_4 as a magnetic because its supermagnetic helps to easy recovery by external magnetic fields which reduce the amount of waste discharged into the environment (Hu, Chen, & Lo, 2005; Hu, Lo, & Chen, 2004; Oliveira et al., 2004; Shin & Jang, 2007; Yavuz et al., 2006). However, due to their high oxidization and instability in various acidic media, Fe_3O_4 MNPs are not very stable under ambient conditions. In addition, the naked Fe_3O_4 MNPs are very susceptible to oxidation in air, which can significantly lose their magnetism and beneficial dispersibility. Fe_3O_4 MNPs should be protected by coating it with a layer to maintain the stability and strength of the individual particles. Inorganic coating materials have shown superiority in nanostructure tuning, good dispersion, ultrafineness, and uniformity.

Among the variety of coating materials, hydroxyapatite (HAp) coating offers a great potential to form a nanocomplex with Fe_3O_4 nanoparticles. The complex structure has made HAp a material with many applications such as high biocompatibility with tissues and cells, so it is studied and applied in many fields such as biomedicine (Manatunga et al., 2017), especially in the field of environmental treatment and improvement (Lin, Pan, Chen, Cheng, & Xu, 2009). It does not only show the ability to treat metals, but also reduce the amount of dissolved organic pollutants when hydroxyapatite is introduced into wastewater samples (Oubagha et al., 2017). However, it also has the disadvantage of having difficulty in separating from the background environment after processing. Therefore, with the remarkable benefits of Fe_3O_4 and the special properties of hydroxyapatite, the combination of these two materials will create a magnetic composite material with outstanding properties while overcoming the limitations of the original materials. Therefore, hydroxyapatite was synthesized from eggshells as the best choice because eggshells are common waste sources that help to limit environmental pollution as well as create valuable materials serving life (Gergely et al., 2010; Thien et al., 2021).

Herein, this study presents the synthesis of Fe_3O_4/HAp adsorbent material from eggshells by-product, and investigates the ability of MB treatment using the as-synthesized material through the average adsorption efficiency, desorption ability, and the maximum adsorption capacity in comparison with other materials.

2. MATERIALS AND METHODS

2.1. Materials

Ferric chloride hexahydrate ($FeCl_3.6H_2O$, 99%), sodium hydroxide (NaOH, 96%), hydrochloric acid (HCl, 36 - 38%), sodium chloride (NaCl, 99.5%), nitric acid (HNO_3, 67%), diammonium phosphate ($(NH_4)_2HPO_4$, 99%) and ammonia solution (NH_4OH, 25 - 28%) purchased from Xilong, China; sodium borohydride ($NaBH_4$, 99%, Merck, Spain), and polyvinylpyrrolidone (PVP, 1 wt%, Sigma-Aldrich, USA), eggshells (GO supermarket, Can Tho). In this study, ethanol (C_2H_5OH, 96%), hydrogen peroxide (H_2O_2, 30%), and distilled (DI) water were obtained from chemical joint stock companies (Southern chemicals joint stock company and Ngan Huong Chemical Co., Ltd.).

2.2. Methods

2.2.1. Adsorbent preparation

Fe_3O_4 nanoparticles were synthesized by wet chemical reduction technique (Chaki et al., 2015). The synthesis process is based on the study Thanh et al. (2021). Briefly, 10 mL $FeCl_3.6H_2O$ 25 mM was added slowly into 20 mL PVP 1% solution, and the mixture was stirred for 10 min with the speed of 400 rpm. Then, 10 mL $NaBH_4$ 125 mM solution was added dropwise into the above mixture, stirred for 30 min under vigorous mechanical stirring at room temperature, constantly. The solution darkens shortly and turns completely black. The obtained Fe_3O_4 nanoparticles were collected by using a permanent magnet, washed many times with distilled water and ethanol until neutral pH, and dried at 60℃ for 2 h.

Preparation $Ca(NO_3)_2$ as the precursor for HAp synthesis. The eggshell powder used in the experiment was pretreated by stripping the membrane off the eggshell, soaking in H_2O_2, rinsing with water, drying, and then fined ground and sifted by Test sieve 0.105 mm to obtain the uniform particles. 60 mL HNO_3 0.5 M solution was added to 1.5 g eggshell powder, which was stirred with the speed of 500 rpm for 1 h under vigorous stirring. After the reaction, the mixture was carried out the filtration, $Ca(NO_3)_2$ 0.25 M solution was obtained. (Nhu, 2021).

The obtained Fe_3O_4 nanoparticles were coated by HAp derived from eggshell powder to maintain the stability and strength of the magnetic nanoparticles.

0.1 g of Fe_3O_4 nanoparticles were suspended in 40 mL $Ca(NO_3)_2$ 0.25 M solution, which was ultrasonically dispersed for 10 minutes. Twenty milliliters of $(NH_4)_2HPO_4$ 0.3 M solution was added dropwise to the Fe_3O_4 suspension under overhead stirring, the pH of the solution was maintained between 10 and 12 by using ammonia solution (Thien et al., 2021). The reaction mixture was further stirred at 90℃ for 2 h and stored for another 12 h (Gu, He, & Wu, 2014). The resulting hydroxyapatite-coated Fe_3O_4 nanoparticles were thoroughly washed with DI water and collected by external magnetic fields, followed by drying at 60℃ for 5 h. The obtained material is referred to as Fe_3O_4/HAp nanoparticles. (Nhu, 2021).

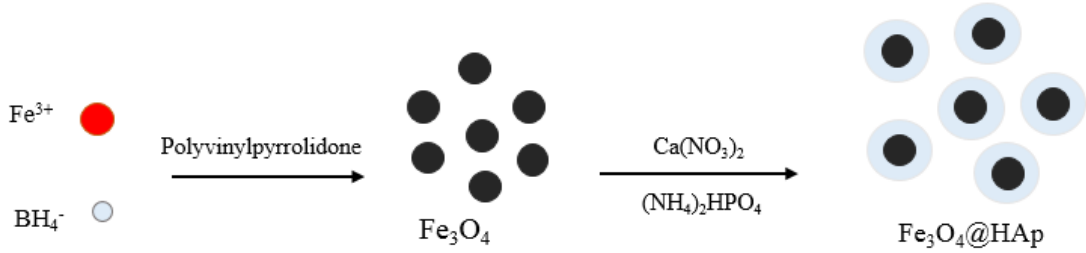

Figure 1. Schematic diagrams of the preparation of Fe_3O_4/HAp sorbent

2.2.2. Adsorbent characterization

Powder X-ray diffraction (XRD) patterns of the nanoparticles were collected on a powder diffraction meter (D2 PHASER, BRUKER, USA), primarily used for phase identification of crystalline material. Fourier transform infrared spectroscopy (FT-IR) determines the presence of functional groups and linkages in the molecule of the adsorbent materials (Agilent FTIR Cary 630 instrument, USA). A high-resolution technique used to reveal structural details, size distribution, and morphology of nanoparticles is transmission electron microscopy (TEM) (JEOL-1010 instrument, Japan). Vibrating sample magnetometer (VSM) (MicroSence EZ9 instrument, USA) was used to determine the magnetic property of Fe_3O_4 and Fe_3O_4/HAp. In addition, ultraviolet-visible (UV-Vis) absorption spectrophotometer (Model Cary 300 UV-VIS Agilent, USA) was used to determine the concentration of MB solution before and after adsorption by Fe_3O_4/HAp.

2.3. Adsorption experiments

For the adsorption experiments, 100 mL MB solution 40 ppm was mixed with 0.5 gram Fe_3O_4/HAp in 4 hours under overhead stirring 200 rpm. During the experiments, the system was continuously stirred, and at the end of the adsorption process, the mixture was separated by using a permanent magnet to obtain two phases. The adsorbent after the adsorption would be further analyzed by FT-IR method while MB concentrations before and after the adsorption experiments were measured by using a double beam UV–Vis spectrophotometer (Model Cary 300 UV-Vis Agilent, USA) at a wavelength of 664 nm. The equilibrium adsorbed concentration, q_e, was calculated according to the equation:

$$q_e = \frac{(C_0 - C_e)V}{M} \quad (1)$$

where C_0 (mmol.L^{-1}) is the initial concentration of MB, C_e (mmol.L^{-1}) is the equilibrium concentration in solution, V (L) is the total volume of solution, and M (g) is the sorbent mass.

2.4. Desorption experiments

For recovery experiments, the used adsorbent was dispersed into 100 mL DI water and stirred under 200 rpm for 3 h at room temperature. The mixture was separated into two phases by using a permanent magnet, the solution was removed while the powder was retained in flask. Then, the synthesized Fe_3O_4/HAp MNPs were dried at 60℃. The recycling material was further confirmed by infrared spectroscopy (FT-IR).

3. RESULTS AND DISCUSSION

3.1. XRD analysis

XRD characterization was employed to further verify the presence of Fe_3O_4 and HAp. The XRD pattern analysis shows the existence of Fe_3O_4 under HAp layer as shown in Figure 2. For Fe_3O_4, diffraction peaks with 2Θ at 30.22°, 35.62°, 42.49°, 53.29°, 57.32°, and 63.01° were observed and in good agreement with the JCPDS No. 19-0629, which are assigned to the corresponding (220), (311), (511), (422), (222) and (004) indices of the cubic inverse spinel structure of pure Fe_3O_4

nanoparticles (Dâas & Hamdaoui, 2010; Han et al., 2014). The stability of the crystalline phase of Fe_3O_4 nanoparticles under HAp coating was confirmed when five characterization peaks of Fe_3O_4 were also observed for Fe_3O_4/HAp spectra. On the other hand, diffraction angles of 25.89°, 31.98°, 32.98°, 34.13°, 39.88°, 46.86°, 49.6°, and 53.35° indicate the appearance of hydroxyapatite layer, which are attributed to (002), (211), (300), (202), (310), (222), (004), and (213), respectively, which belong to HAp (COD No. 96-900-2215), suggesting the formation of HAp phase (Kim, Sambudi, & Cho, 2019). Therefore, it can be seen that Fe_3O_4/HAp is completely formed with Fe_3O_4 MNPs that is enveloped by a HAp layer.

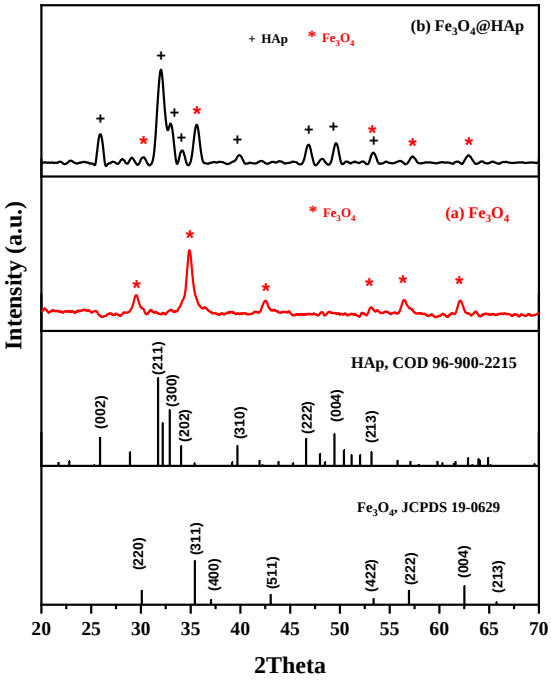

Figure 2. X-ray diffraction patterns of (a) Fe_3O_4 nanoparticles and (b) Fe_3O_4/HAp composites nanoparticles

Additionally, in Fe_3O_4/HAp pattern, peaks of Fe_3O_4 have relatively low intensity value due to their small size and be covered by HAp in comparison with another research (Yang et al., 2010), it can be explained as the result of a thick layer HAp that covering Fe_3O_4 with the morphology of rod-like particles and the reaction condition is far different with simple wet chemical reduction technique for Fe_3O_4 and no calcining step for HAp forming in this study.

3.2. FT-IR analysis

In order to further confirm the presence of functional groups and bonds of Fe_3O_4/HAp, FT-IR spectra were measured. As shown in Figure 3, Fe–O vibration appears the characteristic absorption at 1389 cm^{-1} and at 565 cm^{-1}, which corresponds to the Fe–O bond of bulk magnetite phase on two samples (Dâas & Hamdaoui, 2010). However, these bands result shift to wavenumbers at 564.72 cm^{-1} and 1385 cm^{-1} because of the overlap of HAp-coated forms on the surface of MNPs. Another reason is that a principal effect of finite nanoparticle size is the breaking of bonds for surface atoms that leads the rearrangement of inlocalized electrons on the particle surface. In addition, the split of the bands is attributed to the split of the energy levels of the quantized Fe_3O_4 nanoparticles (Ma et al., 2003).

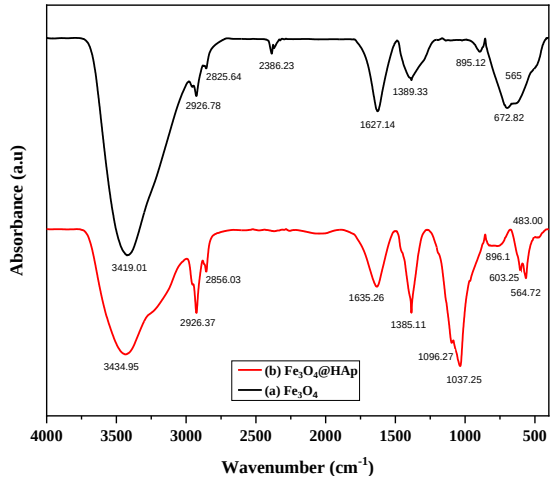

Figure 3. FT-IR spectra of (a) Fe_3O_4, (b) Fe_3O_4/Hap

The new absorption peak of PO_4^{3-}-derive bands were at the wavelengths of 1037.05 cm^{-1} (stretching mode), and at 601–603 cm^{-1} related to the asymmetric P-O vibrations and O-P-O bonds correspondingly were noted at Fe_3O_4/HAp sample (Tanaka et al., 2012). The highlight of this study is that no impured bands, especially CO_3^{2-}derived bands are no observed from FT-IR result though the powdered eggshells were not calcined. Moreover, a broad band observed at 1635.26 cm^{-1} and 1627.14 cm^{-1}, which responds to O–H vibrations recorded at 1626–1637 cm^{-1}, and 3400–3425 cm^{-1} , 2926 cm^{-1} and 2856 cm^{-1} (Chaki et al., 2015) was attributed to the stretching modes of water molecules due to the existence of surface hydroxyl of HAp and DI water used as solvent (S. Yang et al., 2015). The results

verified the formation of calcium hydroxyapatite on the Fe_3O_4 surface, HAp-layer not only maintains the stability and strength of magnetic nanopaticles, but also elevates potential applications of the combined material.

3.3. TEM analysis

The morphology and size of the synthesized Fe_3O_4/HAp composite samples were presented in Figure 4 at different magnification. The TEM images demonstrate that the NPs consist of many ultra-fine particles that agglomerate together to form clusters (Nga et al., 2018). However, at greater magnifications (Fig 4b and 4c), the resulting images are relatively clear in which the composite structure with light contrast HAp layer and dark contrast particle of Fe_3O_4.

The result suggests that Fe_3O_4 were uniform NPs about 10 nm with the nanoparticles are almost spherical in shape, similarly to previous studies (Chaki et al., 2015; Dâas & Hamdaoui, 2010). Besides that, the typical synthesized-HAp were dispersed rod-like particles with about 10 nm in width and 50 nm in length (Gu et al., 2014), part of final material was dispersed in spherical shape (Figure 4c). The morphology of HAp was investigated and resembled the study of Kim et al. (2019) which explains the agglomeration of nano-size rod-like materials by using the wet precipitation method, the magnetic attraction and Van der Waals force among iron oxide were considered (Abidin et al., 2020). In addition, the morphologies of HAp changed from granular to rod-like particles when the pH changed and the temperature increased (Liu et al., 2003). Furthermore, the experimental conditions were not stable so that the final product was not homogeneous, which has HAp rod and sphere in shape in somewhere. Nonetheless, the result was still ensured the HAp-coated on Fe_3O_4 MNPs, it can infer that the hydrophilic Fe_3O_4 MNPs were successfully coated by a HAp shell**.**

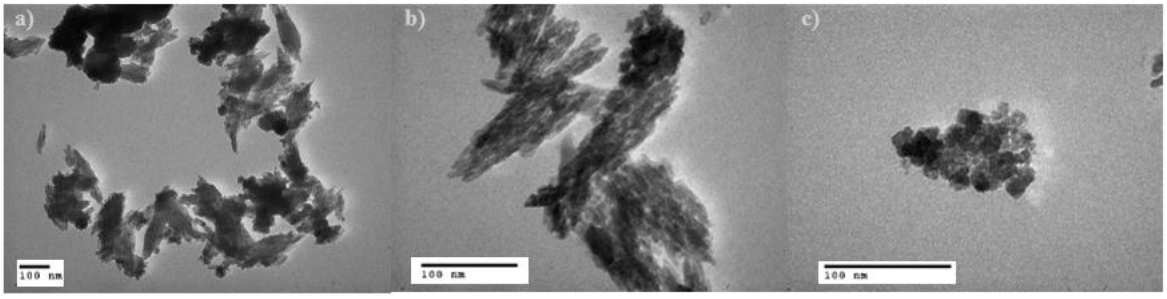

Figure 4. TEM images of Fe_3O_4/HAp nanoparticles with different magnification 20000X (a), 60000X(b) and 80000X (c)

3.4. Magnetization

Magnetic properties of the as-synthesized Fe_3O_4 and Fe_3O_4/HAp samples was studied with the help of VSM, which were shown in Figure 5. From this figure, it is worth noting that the coercive field and remanence magnetization is very small (approximately zero). These are characteristics of super paramagnetic particles (Chaki et al., 2015). The value of saturation magnetization (Ms) is 54.14 $emu.g^{-1}$ for Fe_3O_4, and 16.23 $emu.g^{-1}$ for Fe_3O_4/HAp, respectively. The reduced Ms can be explained by the covering of the HAp surrounding the Fe_3O_4 MNPs, which weakens the magnetic properties when HAp was not magnetic (Z.-p. Yang et al., 2010). In addition, the thick layer of HAp with rod-like shape and uneven dispersion of magnetic NPs relying on TEM images are further reasons that the saturation magnetization of the final material is lower than other studies. Besides, saturation magnetization and coercivity values were also influenced by many factors as crystallite size, microstrain, presence of parasitic phases, cation distribution, interparticle interaction, etc. (Vučinić-Vasić et al., 2019).

Although its Ms reduces, Fe_3O_4/HAp still ensures the superparamagnetic properties and is still sufficiently strong to be magnetically separable when a magnetic field was applied. The result indicates that the superparamagnetic property of the Fe_3O_4/HAP nanoparticles creates a favorable condition for preventing them from aggregation as well as giving them ability to redisperse rapidly when the magnetic field is removed, which is critical for their application in industrial catalysis, environmental protection, biomedical and bioengineering field (Z.-p. Yang et al., 2010).

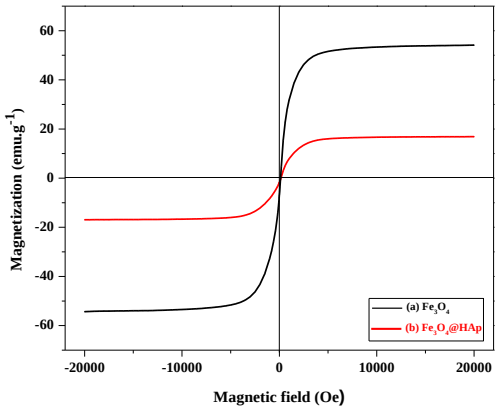

Figure 5. Magnetization curves of (a) Fe_3O_4 NPs, (b) Fe_3O_4/HAp NPs

3.5. Methylene Blue adsorption and desorption

3.5.1. Point of zero point measurements

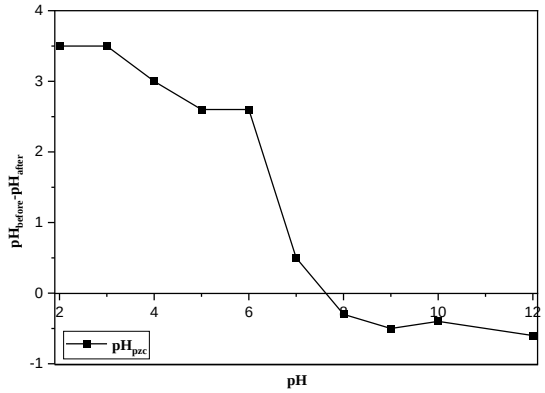

Figure 6. Point of zero charge of Fe_3O_4/HAp nanoparticles

The surface charge measured as point of zero charge is presented in Figure 6 for the Fe_3O_4/HAp nanoparticles. The point of zero charge (pH_{pzc}) of the synthesized-Fe_3O_4/HAp was found to be 7.7 after the measurements. At pH below the pH_{pzc}, the surface of the material is positively charged (Barka et al., 2008; Corami et al., 2008). As mentioned above, the positively charged surface sites on the synthesized material and MB cations have the electrostatic repulsions which do not favor the adsorption. Actually, at the acidic medium, the competition of excess protons (H^+) with MB cations occur for active adsorption sites of Fe_3O_4/HAp could also explain the lower adsorption. On the other hand, at pH values higher than pH_{pzc}, the sorbent surface becomes negatively charged because of the adsorption of OH^- from the solution. It helps to increase in electrostatic attraction forces, acting between the surface and the cations of the adsorbate which contributes to a greater cation sorption at higher pH.

3.5.2. Adsorption efficiency

The experiment of MB removal using Fe_3O_4/HAp was triplicated and the removal efficiency was reported in Table 1. After 40-min reaction, Fe_3O_4/HAp can remove up to 89.6% Methylene Blue, this result is corresponding to the study of Anuar et al. (2019). In addition, the adsorption results were compared with the adsorption yield of Fe_3O_4 at about 45%, HAp is about 50% after 4 hours (Abidin et al., 2020) and Fe_3O_4/HAp was calculated upto 89% from this study. It can be explained as the specific surface area of adsorbent nanoparticles increase, which compared to pure HAp (Abidin et al., 2020; Gu et al., 2014), and Fe_3O_4 MNPs are not stable without HAp coated-layer (Zheltova et al., 2020). Furthermore, this proves that the material has not only physical adsorption but also chemical adsorption, which enhances the adsorption capacity to degrade MB (Abidin et al., 2020)). Indeed, 0.5 g Fe_3O_4/HAp in 40 min stirring, the material can adsorb 40 ppm MB solution with the adsorption efficiency of up to 89.6%, therefore, Fe_3O_4/HAp will be an excellent candidate for adsorption process.

The adsorption ability of Fe_3O_4/HAp on MB can be further confirmed in Figure 7. There are some changes in FT-IR spectra of Fe_3O_4/HAp before and after adsorption process. It could be seen that the stretching vibration adsorption band of hydroxyl groups at 3449 cm^{-1} was broadening as well as the new stretching vibration adsorption bands 1419 - 1470 cm^{-1} were attributed to benzene ring framework from MB (Allam et al., 2016), this proved that MB was adsorbed by related groups of Fe_3O_4/HAp. Moreover, after adsorption, the absorption bands of P-O or O-P-O groups at 1036-1038 cm^{-1} were also broadened. Additionally, hydrogen bond from MB, which forms nitrogen atoms has the propensity for forming hydrogen bond with hydroxyl groups from Fe_3O_4/HAp surface when having awful attracting electron ability and less atom radius. It was reported that a strong H-bonding interaction between P-OH group of HAP particles and N of the MB molecule could contribute to the adsorption of MB molecules (Sharma & Das, 2013). The nitrogen atom of MB might interact with Ca^{2+} groups of HAp via Lewis acid-base interaction (Bouyarmane et al., 2010).

Nevertheless, based on some previous studies on MB adsorption using HAp (Abidin et al., 2020; Allam et al., 2016), the adsorption is mostly a physical process. Due to the porous structure of HAp layer, Methylene Blue molecules have the tendency of passing through the layers of the material at first, then were adsorbed on the surface before diffusing into the porous structure of HAp. Additionally, electrostatic interaction and Van der Waals force have a part in keeping the MB molecules been onto the adsorbent surface. At pH above 8, as mentioned in pH_{pzc} results, the electrostatic attraction between the negative charge of the material and the positive charge of the dye is significant, which leads to increase the percentage of adsorption of the dye onto the surface of the material.

Table 1. MB removal efficiency of Fe_3O_4/HAp

pH	Time (h)	m (mg)	Co (mg.L^{-1})	C_{MB} (mg.L^{-1})	Removal (%)
				4.21	89.5
8	4	500	40	4.25	89.4
				4.08	89.8
Average removal efficiency (%)					**89.6±0.2**

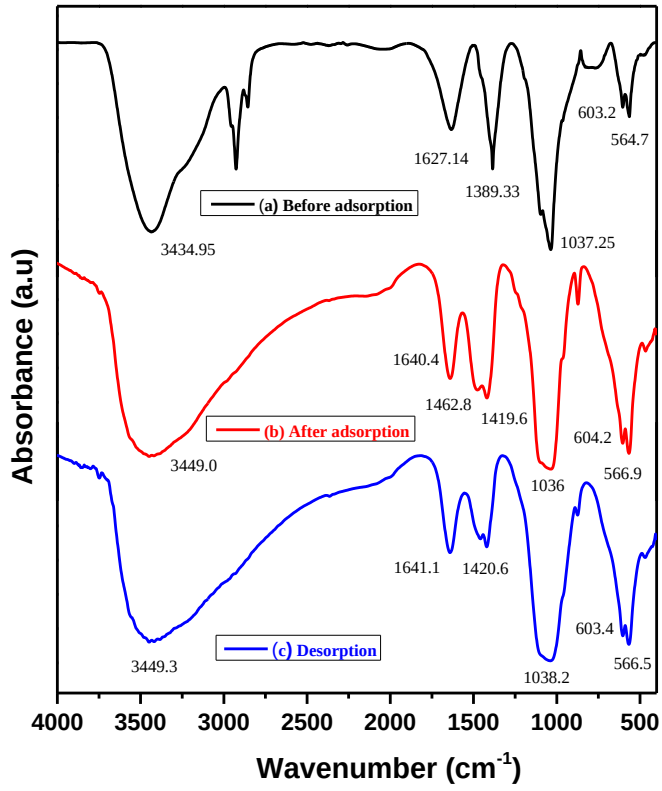

Figure 7. FT-IR spectra of (a) Fe_3O_4/HAp, (b) after adsorption, (c) after desorption

Evaluating the desorption ability, nanomaterials were compared by FT-IR result. The intensity of the stretching vibration adsorption bands 1419-1470 cm^{-1} (benzene ring) significantly decreases since a large amount of concentration of MB was removed by the electrostatic interaction of DI water, and nanoporous was replaced H_2O molecules. This explains for the adsorption bands of O-H were broadener than the original material. In addition, the intensity is not significantly reduced since nano-adsorbent has porous structure, corresponding to a long adsorption time, desorption also takes a long time to desorb completely. Besides, the O-P-O bond at wavenumber 1036 cm^{-1} was expanded, possibly due to MB adsorption process, then the bond of Hap was broken down. It is suggested that the adsorption process is a physical adsorption process based on the Van der Waals electrostatic force.

3.5.3. The maximum adsorption capacity

Adsorption capacity is the amount of adsorbate that is taken up by the adsorbent per unit mass of the adsorbent. Table 2 shows the adsorption capacity of Fe_3O_4/HAp relying on its adsorption process. Furthermore, the adsorbent still gives promising results in removing Methylene Blue, which is around 89.6% in the first process. The removal efficiency decreases to 69.8% in the second process and only 43.5% in the last process. It can be seen that after 3 times adsorption, the adsorption capacity of the material shows a significant drop compared to the first time. Through the results, the maximum adsorption capacity is calculated as q_{max} = 16.4 $mg.g^{-1}$.

Table 3 shows the comparison in maximum adsorption capacity of various adsorption materials used to remove MB under different conditions. The maximum adsorption capacity q_{max} of Fe_3O_4/HAp was higher than that of HAp-Fe_3O_4-100 in previous study (Abidin et al., 2020) with the same reaction conditions. However, when compared with other materials, the maximum adsorption capacity is even lower. It is explained that each material will have various structural components so the adsorption capacity will be different, leading to the different adsorption capacity.

Table 2. Adsorption capacity of Fe_3O_4/HAp

pH	Time (h)	m (mg)	C_o ($mg.L^{-1}$)	C_{MB} ($mg.L^{-1}$)	Removal (%)	q_e ($mg.g^{-1}$)
				4.15	89.6	7.17
8	4	500	40	12.1	69.8	5.76
				22.6	43.5	3.48

Table 3. The comparison in maximum adsorption capacity of various adsorbents for removing MB

Absorbent	pH	Time (h)	m(g)	q_{max} ($mg.g^{-1}$)	References
BC-HAp	8	10	1	21.1	(Li et al., 2018)
Carbon made from Almond Burk	5.7	0.9	0.5	76.3	(Rahimian & Zarinabadi, 2020)
CuO-A	7	3.5	0.4	36.5	(Saruchi et al., 2019)
HAp-Fe_3O_4-100	-	4	0.5	12.4	(Abidin et al., 2020)
Fe_3O_4/HAp	8	4	0.5	16.4	This work

4. CONCLUSIONS

The successful synthesis of Fe_3O_4/HAp nanoparticles from eggshells and its adsorption capacity for MB from aqueous solution are reported. HAp synthesized from eggshell by-products was successfully coated on Fe_3O_4 MNPs with a simple, easy and optimized process. In addition, using eggshell by-products is considered a solution for reducing significantly waste into the environment. The characteristic results show that Fe_3O_4/HAp nanoparticles were successfully synthesized by wet precipitation from available materials, the morphology and size of absorbent relatively small, and superparamagnetic property of the Fe_3O_4/HAp nanoparticles are still ensured which is suitable for the adsorption process. Lastly, at contact time of 40 min, initial MB concentration of 40 ppm, 0.5 g of material and pH 8, the maximum adsorption efficiency was 89.6%, and maximum adsorption capacity was calculated as 16.4 $mg.g^{-1}$.

ACKNOWLEDGMENT

This work was supported by the Scientific Research Projects Coordination Unit of Can Tho University (code: THS2021-13). The authors thank the Department of Chemical Engineering of Can Tho University for some analyses.

REFERENCES

Abidin, N. H. Z., Sambudi, N. S., & Kamal, N. A. (2020). Composite of Hydroxyapatite-Fe3O4 for the Adsorption of Methylene Blue. *ASEAN Journal of Chemical Engineering, 20*(2), 140-153.

Allam, K., El Bouari, A., Belhorma, B., & Bih, L. (2016). Removal of methylene blue from water using hydroxyapatite submitted to microwave irradiation. *Journal of Water Resource and Protection, 8*(3), 358-371.

Barka, N., Qourzal, S., Assabbane, A., Nounah, A., & Yhya, A.-I. (2008). Adsorption of Disperse Blue SBL dye by synthesized poorly crystalline hydroxyapatite. *Journal of Environmental Sciences, 20*(10), 1268-1272.

Bouyarmane, H., El Asri, S., Rami, A., Roux, C., Mahly, M., Saoiabi, A., . . . Laghzizil, A. (2010). Pyridine and phenol removal using natural and synthetic apatites as low cost sorbents: influence of porosity and surface interactions. *Journal of Hazardous Materials, 181*(1-3), 736-741.

Chaki, S., Malek, T. J., Chaudhary, M., Tailor, J., & Deshpande, M. (2015). Magnetite Fe3O4 nanoparticles synthesis by wet chemical reduction and their characterization. *Advances in Natural Sciences: Nanoscience and Nanotechnology, 6*(3), 035009.

Corami, A., Mignardi, S., & Ferrini, V. (2008). Cadmium removal from single-and multi-metal (Cd+ Pb+ Zn+ Cu) solutions by sorption on hydroxyapatite. *Journal of colloid and interface science, 317*(2), 402-408.

Dâas, A., & Hamdaoui, O. (2010). Extraction of anionic dye from aqueous solutions by emulsion liquid membrane. *Journal of Hazardous Materials, 178*(1-3), 973-981.

El-Gohary, F., & Tawfik, A. (2009). Decolorization and COD reduction of disperse and reactive dyes wastewater using chemical-coagulation followed by sequential batch reactor (SBR) process. *Desalination, 249*(3), 1159-1164.

El-Naas, M. H., Al-Muhtaseb, S. A., & Makhlouf, S. (2009). Biodegradation of phenol by Pseudomonas putida immobilized in polyvinyl alcohol (PVA) gel. *Journal of Hazardous Materials, 164*(2-3), 720-725.

Gergely, G., Wéber, F., Lukács, I., Tóth, A. L., Horváth, Z. E., Mihály, J., & Balázsi, C. (2010). Preparation and characterization of hydroxyapatite from eggshell. *Ceramics international, 36*(2), 803-806.

Gomes, H. T., Machado, B. F., Ribeiro, A., Moreira, I., Rosário, M., Silva, A. M., . . . Faria, J. L. (2008). Catalytic properties of carbon materials for wet oxidation of aniline. *Journal of Hazardous Materials, 159*(2-3), 420-426.

Gu, L., He, X., & Wu, Z. (2014). Mesoporous Fe3O4/hydroxyapatite composite for targeted drug delivery. *Materials Research Bulletin, 59*, 65-68.

Han, R., Li, W., Pan, W., Zhu, M., Zhou, D., & Li, F.-s. (2014). 1D magnetic materials of Fe 3 O 4 and Fe with high performance of microwave absorption fabricated by electrospinning method. *Scientific reports, 4*(1), 1-5.

Hu, J., Chen, G., & Lo, I. M. (2005). Removal and recovery of Cr (VI) from wastewater by maghemite nanoparticles. *Water research, 39*(18), 4528-4536.

Hu, J., Lo, I., & Chen, G. (2004). Removal of Cr (VI) by magnetite. *Water Science and Technology, 50*(12), 139-146.

Kim, J., Sambudi, N. S., & Cho, K. (2019). Removal of Sr2+ using high-surface-area hydroxyapatite synthesized by non-additive in-situ precipitation. *Journal of environmental management, 231*, 788-794.

Li, Y., Zhang, Y., Wang, G., Li, S., Han, R., & Wei, W. (2018). Reed biochar supported hydroxyapatite nanocomposite: Characterization and reactivity for methylene blue removal from aqueous media. *Journal of Molecular Liquids, 263*, 53-63.

Lin, K., Pan, J., Chen, Y., Cheng, R., & Xu, X. (2009). Study the adsorption of phenol from aqueous solution on hydroxyapatite nanopowders. *Journal of Hazardous Materials, 161*(1), 231-240.

Liu, J., Ye, X., Wang, H., Zhu, M., Wang, B., & Yan, H. (2003). The influence of pH and temperature on the morphology of hydroxyapatite synthesized by hydrothermal method. *Ceramics international, 29*(6), 629-633.

Ma, M., Zhang, Y., Yu, W., Shen, H.-y., Zhang, H.-q., & Gu, N. (2003). Preparation and characterization of magnetite nanoparticles coated by amino silane. *Colloids and Surfaces A: physicochemical and engineering aspects, 212*(2-3), 219-226.

Manatunga, D. C., de Silva, R. M., de Silva, K. N., de Silva, N., Bhandari, S., Yap, Y. K., & Costha, N. P. (2017). pH responsive controlled release of anti-cancer hydrophobic drugs from sodium alginate and hydroxyapatite bi-coated iron oxide nanoparticles. *European Journal of Pharmaceutics and Biopharmaceutics, 117*, 29-38.

Nga, N. K., Chau, N. T. T., & Viet, P. H. (2018). Facile synthesis of hydroxyapatite nanoparticles mimicking biological apatite from eggshells for bone-tissue engineering. *Colloids and Surfaces B: Biointerfaces, 172*, 769-778.

Nhu, L. T. Q. (2021). *Synthesis of magnatic nanoparticles Fe_3O_4@HAp with HA derived from blood cockle's shell and its application for Cr(VI) adsorption from synthetic wastewater.* Can Tho University, College of Engineering Technology.

Oliveira, L. C., Petkowicz, D. I., Smaniotto, A., & Pergher, S. B. (2004). Magnetic zeolites: a new adsorbent for removal of metallic contaminants from water. *Water research, 38*(17), 3699-3704.

Oubagha, N., Lemlikchi, W., Sharrock, P., Fiallo, M., & Mecherri, M. O. (2017). Hydroxyapatite precipitation with Hydron Blue dye. *Journal of environmental management, 203*, 807-810.

Rahimian, R., & Zarinabadi, S. (2020). A review of studies on the removal of methylene blue dye from industrial wastewater using activated carbon adsorbents made from almond bark. *Progress in Chemical and Biochemical Research, 3*(3), 251-268.

Saruchi, Thakur, P., & Kumar, V. (2019). Kinetics and thermodynamic studies for removal of methylene blue dye by biosynthesize copper oxide nanoparticles and its antibacterial activity. *Journal of Environmental Health Science and Engineering, 17*(1), 367-376. doi:10.1007/s40201-019-00354-1

Sharma, P., & Das, M. R. (2013). Removal of a cationic dye from aqueous solution using graphene oxide

nanosheets: investigation of adsorption parameters. *Journal of Chemical & Engineering Data, 58*(1), 151-158.

Shin, S., & Jang, J. (2007). Thiol containing polymer encapsulated magnetic nanoparticles as reusable and efficiently separable adsorbent for heavy metal ions. *Chemical communications*(41), 4230-4232.

Tanaka, H., Tsuda, E., Nishikawa, H., & Fuji, M. (2012). FTIR studies of adsorption and photocatalytic decomposition under UV irradiation of dimethyl sulfide on calcium hydroxyapatite. *Advanced Powder Technology, 23*(1), 115-119.

Thanh, L. H. V., Han, K. G., Han, N. N., Pha, B. Y., & Ngoc, M. N. T. (2021). Tổng hợp vật liệu Fe3O4@ SiO2 đính Fe0 và xử lý methyl blue trong nước. *Tạp chí Khoa học Trường Đại học Cần Thơ, 57*(4), 40-52.

Thien, D. V. H., Thuyen, N. T. B., Quyen, T. T. B., Chiem, N. H., & Viet, P. H. (2021). Microwave-assisted synthesis of nanorod hydroxyapatite from eggshells. *Vietnam Journal of Science, Technology and Engineering, 63*(1), 3-6.

Vučinić-Vasić, M., Antić, B., Bošković, M., Antić, A., & Blanuša, J. (2019). Hydroxyapatite/iron oxide nanocomposite prepared by high energy ball milling. *Processing and Application of Ceramics, 13*(2), 210-217.

Wu, T., Cai, X., Tan, S., Li, H., Liu, J., & Yang, W. (2011). Adsorption characteristics of acrylonitrile, p-toluenesulfonic acid, 1-naphthalenesulfonic acid and methyl blue on graphene in aqueous solutions. *Chemical Engineering Journal, 173*(1), 144-149.

Yang, S., Zeng, T., Li, Y., Liu, J., Chen, Q., Zhou, J., . . . Tang, B. (2015). Preparation of graphene oxide decorated Fe3O4@ SiO2 nanocomposites with superior adsorption capacity and SERS detection for organic dyes. *Journal of Nanomaterials, 2015*.

Yang, Z.-p., Gong, X.-y., & Zhang, C.-j. (2010). Recyclable Fe3O4/hydroxyapatite composite nanoparticles for photocatalytic applications. *Chemical Engineering Journal, 165*(1), 117-121.

Yavuz, C. T., Mayo, J., William, W. Y., Prakash, A., Falkner, J. C., Yean, S., . . . Tomson, M. (2006). Low-field magnetic separation of monodisperse Fe3O4 nanocrystals. *science, 314*(5801), 964-967.

Zheltova, V., Vlasova, A., Bobrysheva, N., Abdullin, I., Semenov, V., Osmolowsky, M., . . . Osmolovskaya, O. (2020). Fe3O4@ HAp core–shell nanoparticles as MRI contrast agent: Synthesis, characterization and theoretical and experimental study of shell impact on magnetic properties. *Applied Surface Science, 531*, 147352.